ACS Photonics

pubs.acs.org/journal/apchd5

Article

Nonreciprocal Thermophotovoltaic Systems

Yubin Park,* Zunaid Omair, and Shanhui Fan*

Cite This: https://doi.org/10.1021/acsphotonics.2c01308

Read Online

ACCESS | Metrics & More | Article Recommendations

ABSTRACT: Thermophotovoltaic systems, like all thermal engines, are constrained by the trade-off between efficiency and power density. Standard thermophotovoltaic systems can have efficiency approaching the Carnot limit only when the power density approaches zero. Here, we propose a nonreciprocal thermophotovoltaic system consisting of multiple nonreciprocal photovoltaic layers. With an infinite number of nonreciprocal photovoltaic layers, our engine can operate at the Carnot efficiency while generating nonzero power. Furthermore, we show that with a finite number of layers, nonreciprocal thermophotovoltaic systems can significantly outperform their reciprocal counterparts. Our work points to the opportunities of exploiting nonreciprocity in thermophotovoltaic systems.

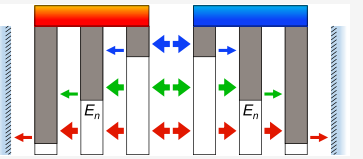

KEYWORDS: *thermophotovoltaics, nonreciprocity, Carnot efficiency*

INTRODUCTION

A thermophotovoltaic (TPV) system is an energy harvesting system that converts a temperature gradient into electricity through a photovoltaic (PV) process.[1−17] It consists of a hot emitter that radiates light and a relatively cold PV cell that receives the thermal radiation and generates electrical power. Over the past few years, there has been significant improvement in the efficiencies of experimentally demonstrated TPV systems.[18−20] In particular, it has been shown that the use of multijunction PV cells with multiple band gaps can considerably enhance the efficiency of TPV systems.[21] (We note that the efficiencies of refs 18−21 are the "pairwise" efficiencies according to the definition of efficiency in ref 22.)

For the design of any thermal engine, the fundamental question is to understand its theoretical efficiency limit and to elucidate the behavior of the engine as its efficiency approaches the theoretical limit. For a TPV system, high efficiency can be reached with the use of a thermal emitter that generates a narrow-band thermal radiation with its frequency matching the band gap of the semiconductor PV cell. In particular, the Carnot efficiency can be attained when the bandwidth of the emitter approaches zero.[2] However, in this case, the generated power density also approaches zero. Therefore, an open theoretical question is to design a TPV system that can maintain high power density while its efficiency approaches the Carnot limit.[23,24]

In this paper, we propose a TPV system that consists of multilayered nonreciprocal PV cells placed on both the hot and the cold side of the TPV system (Figure 1a) and investigate the theoretical limits to the performance. We show that in the limit of an infinite number of layers, the system can operate at the Carnot efficiency with nonzero power density. Moreover, the system can maintain both high efficiency and high power density with a finite number of layers.

Our work is related to ref 25, which showed that in solar energy harvesting the Landsberg limit can be reached by a multilayered nonreciprocal PV cell. Compared with the ref 25, here we place the PV cells on both the hot and the cold side of the heat engine, as is appropriate for a TPV system. Our work is also related to the work of Buddhiraju et al., who showed that the Carnot limit can be reached for thermal energy harvesting at maximum power.[26] Reference 26 utilized a configuration consisting of Carnot engines and optical circulators. Our configuration based on nonreciprocal PV cells is more compact and more readily implementable. All these works, including our present paper and the earlier works, emphasize the essential role that nonreciprocity plays in reaching the theoretical limit of energy harvesting.[25−30]

NONRECIPROCAL TPV SYSTEM

Figure 1a shows the illustration of our nonreciprocal TPV system. Each bar labeled as n, where $n = 1, 2, ..., M$, represents a layer of PV cell with band gap E_n. We assume $E_1 < E_2 < \cdots < E_M$. The PV cells are placed on the hot side as well as the cold side, M layers each. Every layer on the hot side is in thermal contact with a thermal bath at temperature T_H, and thus, their temperatures are maintained at T_H. Similarly, the temperatures of the cold side layers are set to T_L.

In this work, for the PV layers, we refer to the design of a semitransparent nonreciprocal absorber proposed in ref 31. Light transport properties of a single layer are shown in Figure

Received: August 22, 2022

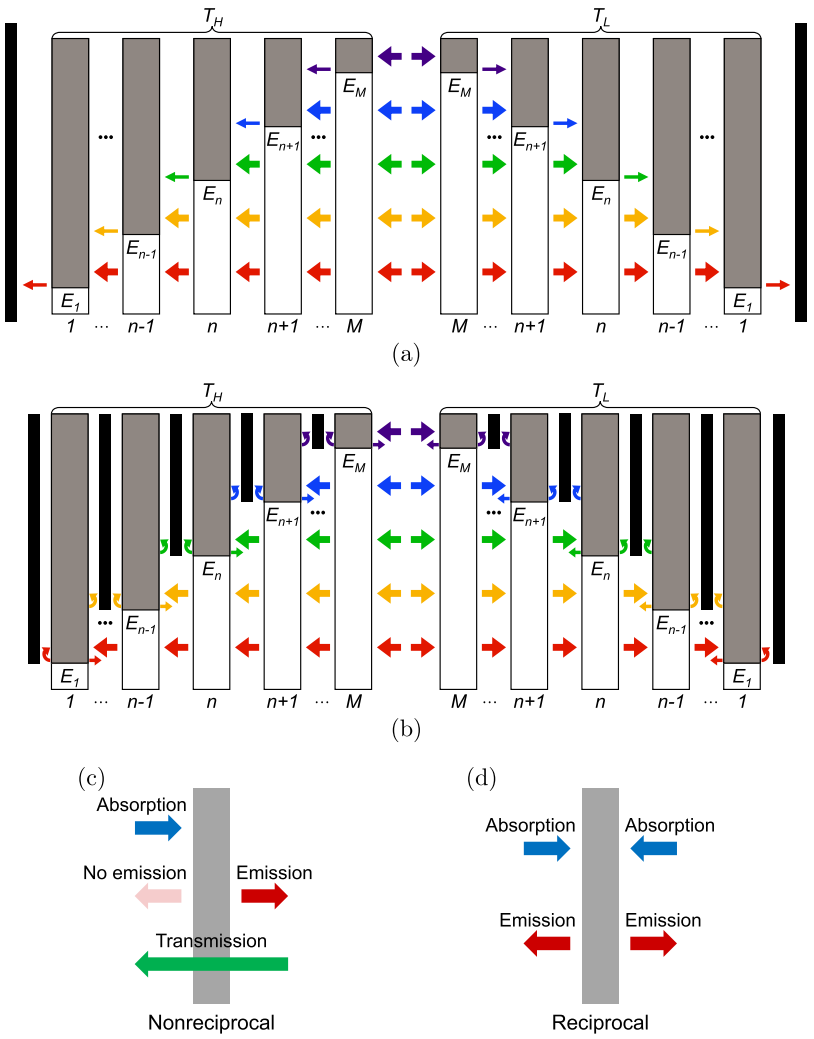

Figure 1. (a) Our nonreciprocal multijunction TPV system. (b) Reciprocal counterpart of our nonreciprocal TPV system. In (a) and (b), each bar represents a PV layer, where the height of the white area indicates its band gap. Each arrow represents light traveling in its direction with energy corresponding to its vertical position. Thick arrows represent light originating from the other side of the TPV system, and thin arrows indicate light emitted from the PV layers. (c, d) Light transport properties of a nonreciprocal PV layer (c) and a reciprocal PV layer (d).

1c. Light incident from one side with energy above the band gap is completely absorbed, and the emission from the layer goes entirely to the opposite side. Then, according to ref 31, in order to satisfy the second law of thermodynamics and the balance of energy flows under thermal equilibrium, light incident from the opposite side has to be completely transmitted through the layer without absorption. Reference 31 has shown that such a nonreciprocal system can be implemented by the use of magneto-optical materials. We also assume that these layers have no nonradiative recombination.

For a description of the operating mechanism of the system, we look at the cold side first. Radiation from the hot side is incident upon the leftmost layer (the Mth layer) on the cold side. The nth layer on the cold side absorbs photons with energy above E_n incident from the left and emits photons with energy above E_n to the right. The emitted photons from the rightmost layer (the first layer) are reflected by a perfect mirror (black rectangle) and travel through all the nonreciprocal PV cell layers on the cold side without absorption, to reach the hot side of the system. On the hot side, the layer configuration and the photon transport process are a mirror image of those on the cold side. We assume that the electric power is extracted from every layer if possible, and the total power is the sum of the power from all the layers.

For this system, we first analyze the case of $M = \infty$, in which the band gap energy E and operating voltages change continuously between consecutive PV layers. We consider energy E starting from zero and continuously increasing up to infinity, and we define $V_H(E)$ and $V_L(E)$ as operating voltages of the PV layers with band gap E on the hot and the cold side, respectively. $V_H(0)$ is the operating voltage of the leftmost hot side layer, and $V_L(0)$ is the operating voltage of the rightmost cold side layer. Note that as pointed out by Buddhiraju et al.,[26] at optimal power generation, the cold side of the TPV system operates under "positive illumination", while the hot side operates under "negative illumination".[32−34] The power-generating mechanism of the hot side is also referred to as "thermoradiative effect" in many references, as a counterpart to the "thermophotovoltaic effect" of the cold side.[35] On the cold side PV layers, the photon absorption rate exceeds the emission rate, which generates a current flow, and the PN-junction of a PV cell is forward biased. On the hot side PV layers, the emission rate exceeds the absorption rate, which causes the current to flow in the opposite direction and the

https://doi.org/10.1021/acsphotonics.2c01308
ACS Photonics XXXX, XXX, XXX−XXX

PN-junction is reverse biased. In this work, we follow the sign convention where a positive voltage corresponds to a forward bias in the PN-junction of a PV cell, and a positive current corresponds to a flow of an external current from the P to the N regions. Therefore, with our sign convention, the currents and voltages of the layers on the cold side are non-negative, while those of the hot side are nonpositive.

First, we focus on the cold side. The photon flux that the cold side receives from the hot side originates from the leftmost layer of the hot side and has the following spectrum, per unit energy interval:

$$n_L(E) = \frac{2\pi}{h^3c^2}\frac{E^2}{\exp\left(\frac{E - qV_H(0)}{kT_H}\right) - 1} \tag{1}$$

where h, c, and k are the Planck constant, the speed of light in vacuum, and the Boltzmann constant, respectively. Therefore, high $V_H(0)$ increases the photon flux, which is advantageous for enhancing the current collected from the cold side PV layers. Since the voltages of the layers on the hot side are nonpositive, we start by setting $V_H(0) = 0$, and we will later show that this choice is consistent from a power optimization point of view. Under this condition, finding $V_L(E)$ as a function of E that maximizes the cold side power is identical to the procedure introduced by Park et al., where efficiency-maximizing condition of a nonreciprocal infinite-junction solar cell is determined.[25] This leads to the following result:

$$V_L(E) = \frac{E}{q}\left(1 - \frac{T_L}{T_H}\right) \tag{2a}$$

$$W_L = \sigma\left(T_H^4 - \frac{4}{3}T_H^3T_L + \frac{1}{3}T_L^4\right) \tag{2b}$$

where q is the elementary charge, σ is the Stefan–Boltzmann constant, and W_L is the total power output from the cold side PV layers. Note that $V_L(0)$ in this case is zero, as a result of power maximization on the cold side.

We now move on to the hot side. The photon flux that the hot side PV layers receive is from the rightmost layer of the cold side and has the following spectrum, per unit energy interval:

$$n_H(E) = \frac{2\pi}{h^3c^2}\frac{E^2}{\exp\left(\frac{E - qV_L(0)}{kT_L}\right) - 1} \tag{3}$$

The hot side operates under negative illumination with nonpositive currents, which results in electric power extraction from the net emitted photon flux. From the optimization of the cold side as determined above, we set $V_L(0) = 0$. Then, $V_H(E)$ that maximizes the hot side power under this condition can be determined by following similar steps to those for finding $V_L(E)$. This leads to the following result:

$$V_H(E) = \frac{E}{q}\left(1 - \frac{T_H}{T_L}\right) \tag{4a}$$

$$W_H = \sigma\left(T_L^4 - \frac{4}{3}T_HT_L^3 + \frac{1}{3}T_H^4\right) \tag{4b}$$

where W_H is the total power output from the hot side PV layers. Note that $V_H(0)$ is zero, as a result of the optimization of the hot side. Thus, our initial setting of $V_H(0) = 0$ is self-consistent from the power optimization point of view.

Since the operating conditions that maximize the power output from the cold side and the hot side are consistent with each other, eqs 2a and 4a are the operating voltages as functions of E that maximize the total power output from the TPV system of Figure 1a. The total power that this TPV system produces under this condition is

$$W = W_L + W_H = \frac{4}{3}\sigma(T_H^3 - T_L^3)(T_H - T_L) \tag{5}$$

We now calculate the TPV efficiency corresponding to this power-maximizing condition. TPV efficiency is calculated by normalizing the output electric power against the total heat that all the hot side PV layers receive from the thermal bath to maintain their temperatures. Following the method of Li et al.,[15] this normalization factor can be calculated by applying the thermal balance equation to each of the hot side PV layers. This leads to the following result:

$$Q_H = \frac{4}{3}\sigma(T_H^3 - T_L^3)T_H \tag{6}$$

Then, the corresponding efficiency is

$$\eta = \frac{W}{Q_H} = 1 - \frac{T_L}{T_H} \tag{7}$$

which is the Carnot efficiency of an engine operating between T_H and T_L.

Equations 5 and 7 show that the nonreciprocal TPV system of Figure 1a can achieve nonzero power generation at the Carnot efficiency when an infinite number of layers are used. For finite systems, from fundamental thermodynamic considerations, one should expect that Carnot efficiency can be exactly reached only when the generated power is zero.[24] Nevertheless, our result on an infinite system points to a potential performance improvement that nonreciprocity can bring to TPV systems that consist of a finite number of layers as well. Below we illustrate such improvement.

COMPARISON TO RECIPROCAL TPV SYSTEMS

We first introduce a configuration of a reciprocal TPV system, shown in Figure 1b, that can be a reasonable counterpart of our nonreciprocal TPV system. The reciprocal TPV system of Figure 1b is related to a multijunction solar PV system proposed by Martí and Araújo[36] and is similar in structure to our nonreciprocal TPV system of Figure 1a except for two differences. First, every PV layer is reciprocal, meaning that the layer satisfies Kirchhoff's law and the absorptivity of the layer for light from one side is equal to the emissivity of the layer to the same side (Figure 1d). Second, low-pass energy filters are placed between adjacent PV layers. The threshold of the filter between the nth and $(n - 1)$th layer is E_n. Therefore, photons with energy higher than E_n are reflected back to where they were emitted from, as shown by thin curved arrows neighboring each black filter in Figure 1b. The use of these low-pass filters prevents the photons emitted from the nth layer from going to the $(n - 1)$th layer where the band gap is E_{n-1} and allows these photons to be reabsorbed by the nth layer where the band gap E_n is higher than E_{n-1}. This leads to higher power output compared to the configuration without the filters.[36] Due to these differences, thermal radiation absorbed by the nth cold side layer originates from the nth hot side layer.

https://doi.org/10.1021/acsphotonics.2c01308
ACS Photonics XXXX, XXX, XXX−XXX

Likewise, the nth hot side layer absorbs the photons emitted from the nth cold side layer. In other words, heat transfer only occurs between hot side and cold side layers of the same band gap.

We then compare the performance of our nonreciprocal TPV system (Figure 1a) to that of the reciprocal TPV system (Figure 1b) for varying number of PV layers, from the single-layered case ($M = 1$) to the infinite-layered case ($M = \infty$). As aforementioned, efficiency by itself is not an ideal way to evaluate the performance of a TPV system, and it is important to consider both efficiency and power output simultaneously. Thus, here we find the power-maximizing conditions and compare the resulting optimal power output as well as the efficiency when the maximum power is achieved. We note that while we aim for power maximization, we avoid the thermophotonic operation of the TPV systems to focus solely on the effect of nonreciprocity.[37] We therefore impose a constraint that power output from each PV layer, both on the hot side and the cold side, is non-negative.

We set T_L to a room temperature of 300 K and T_H to 1500 K, which are reasonable values for TPV systems.[18−21,38,39] We note that here for illustration purpose we assume that the hot side has a temperature of 1500 K. In practice, many PV cells may no longer operate properly at such a high temperature. Our design, on the other hand, is applicable when the hot side temperature is significantly lower as well. We consider the case in which there are M number of layers on each side of the TPV system. In this case, the variables that we can tune are the band gaps (E_1, E_2, ..., E_M), operating voltages of the hot side layers (V_{H1}, V_{H2}, ..., V_{HM}), and operating voltages of the cold side layers (V_{L1}, V_{L2}, ..., V_{LM}).

Power maximization is conducted following the efficiency maximization process of Park et al.[25] or Brown and Green.[40] Current collected at each layer can be calculated from the difference between absorbed and emitted photon flux. Then, power generated from each layer is simply the collected current multiplied by the operating voltage of the layer. The total power output from the system is the sum of power from every layer. We find optimal conditions of band gaps and operating voltages so that the total generated power is maximized. After finding the power-maximizing condition, we work out the efficiency corresponding to this condition, following a procedure similar to that used for deriving eqs 6 and 7.

For the case with an infinite number of layers, the result for the nonreciprocal TPV system has been already shown in eqs 5 and 7. For the reciprocal system, calculation similar to that of Brown and Green[40] or Vos[41] can be done to work out the maximum power and corresponding efficiency.

Figure 2 shows the result summarizing the maximum power and efficiency calculation above. Each point on the solid-line plots represents a case with a finite number of layers. The most bottom-left data point is the single-layered case ($M = 1$). In this case, performances of the nonreciprocal and reciprocal TPV system are equal because with one layer on each side the effects of the photon transfer processes are essentially identical. As the number of layers increases, both the power and the efficiency increase, as shown in Figure 2. Both the power and the efficiency reach the maximum with an infinite number of layers. As mentioned above, for our nonreciprocal TPV system, the efficiency at the infinite-layer limit is the Carnot efficiency. On the other hand, the reciprocal system does not reach the Carnot efficiency even in the infinite-layer limit. We stress that other than the single-layered case, nonreciprocal TPV systems always outperform the reciprocal counterparts in terms of both maximum power and corresponding efficiency. Especially in the infinite limit, the nonreciprocal system produces 1.8 times more power than the reciprocal system. Data of maximum power outputs and efficiencies for $M = 1, 2, 3, \infty$, are organized in Tables 1 and 2, together with corresponding optimal band gaps and operating voltages.

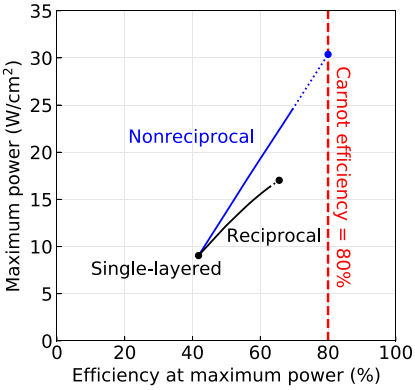

Figure 2. Plot of maximum power vs corresponding efficiency for nonreciprocal TPV systems and reciprocal counterparts (T_H = 1500 K, T_L = 300 K). Each point on the solid-line plots represents a case with a finite number of layers. The bottom-left is the single-layered case, and the corresponding number of layers increases as we move in the upper-right direction of the solid-line plot. The points on the most right show the result for infinite-layered cases.

Optimization conducted aiming for power maximization tends to prefer thermophotonic operation of the system, where the operating voltages of the hot side PV layers are positive, resulting in increased light emission from the hot side and higher power generation from the cold side. These thermophotonic systems are known for operating with significantly high power density.[37] In such thermophotonic operation, the PV layers on the hot side consume rather than produce power. However, as discussed above, we have imposed a constraint for avoiding thermophotonic operation by requiring power output from each layer to be non-negative. In our case, power maximization ends up pushing the hot side operating voltages to zero, which is the upper bound we set. In the nonreciprocal TPV system of Figure 1a, photon flux that every cold side PV layer receives from the hot side originates from the leftmost layer of the hot side. Therefore, among the hot side operating voltages V_{H1}, V_{H2}, ..., V_{HM}, only V_{H1} of the leftmost layer is involved in the calculation of power output from the cold side. In the reciprocal case of Figure 1b, however, the photon flux that the nth cold side layer absorbs originates from the nth hot side layer only and, thus, is determined by V_{Hn} of the nth hot side layer. As a result, for the nonreciprocal case, only V_{H1} is pushed to zero under power-maximizing conditions (Table 1), but for the reciprocal case, every hot side operating voltage is (Table 2). Consequently, for $M \geq 2$, power is only generated from the cold side in the reciprocal case, but from both sides in the nonreciprocal case. This is why the maximum power values that we attain with nonreciprocal TPV systems exceed those of reciprocal TPV systems for $M \geq 2$. Note also that power maximization of a reciprocal TPV system follows the same optimization process as that for efficiency maximization of a multijunction solar cell[40] because all the hot side operating voltages end up being zero.

https://doi.org/10.1021/acsphotonics.2c01308
ACS Photonics XXXX, XXX, XXX−XXX

Table 1. Data of Band Gaps, Operating Voltages, Maximum Powers, and Efficiencies of Our Nonreciprocal TPV Systems (Figure 1a) under Power-Maximizing Conditions for T_H = 1500 K and T_L = 300 K

	band gaps (eV)			operating voltages (V)							
M	E_1	E_2	E_3	V_{H1}	V_{H2}	V_{H3}	V_{L1}	V_{L2}	V_{L3}	max power (W/cm^2)	eff (%)
1	0.27			0			0.22			9.0	41.8
2	0.16	0.33		0	−0.13		0.13	0.27		14.0	50.6
3	0.11	0.21	0.41	0	−0.10	−0.23	0.09	0.18	0.33	17.1	56.0
∞										30.4	80.0

Table 2. Data of Band Gaps, Operating Voltages, Maximum Powers, and Efficiencies of Reciprocal TPV Systems (Figure 1b) under Power-Maximizing Conditions for T_H = 1500 K and T_L = 300 K

	band gaps (eV)			operating voltages (V)							
M	E_1	E_2	E_3	V_{H1}	V_{H2}	V_{H3}	V_{L1}	V_{L2}	V_{L3}	max power (W/cm^2)	eff (%)
1	0.27			0			0.22			9.0	41.8
2	0.18	0.43		0	0		0.15	0.33		12.2	49.8
3	0.14	0.32	0.55	0	0	0	0.12	0.24	0.42	13.7	54.2
∞										17.0	65.6

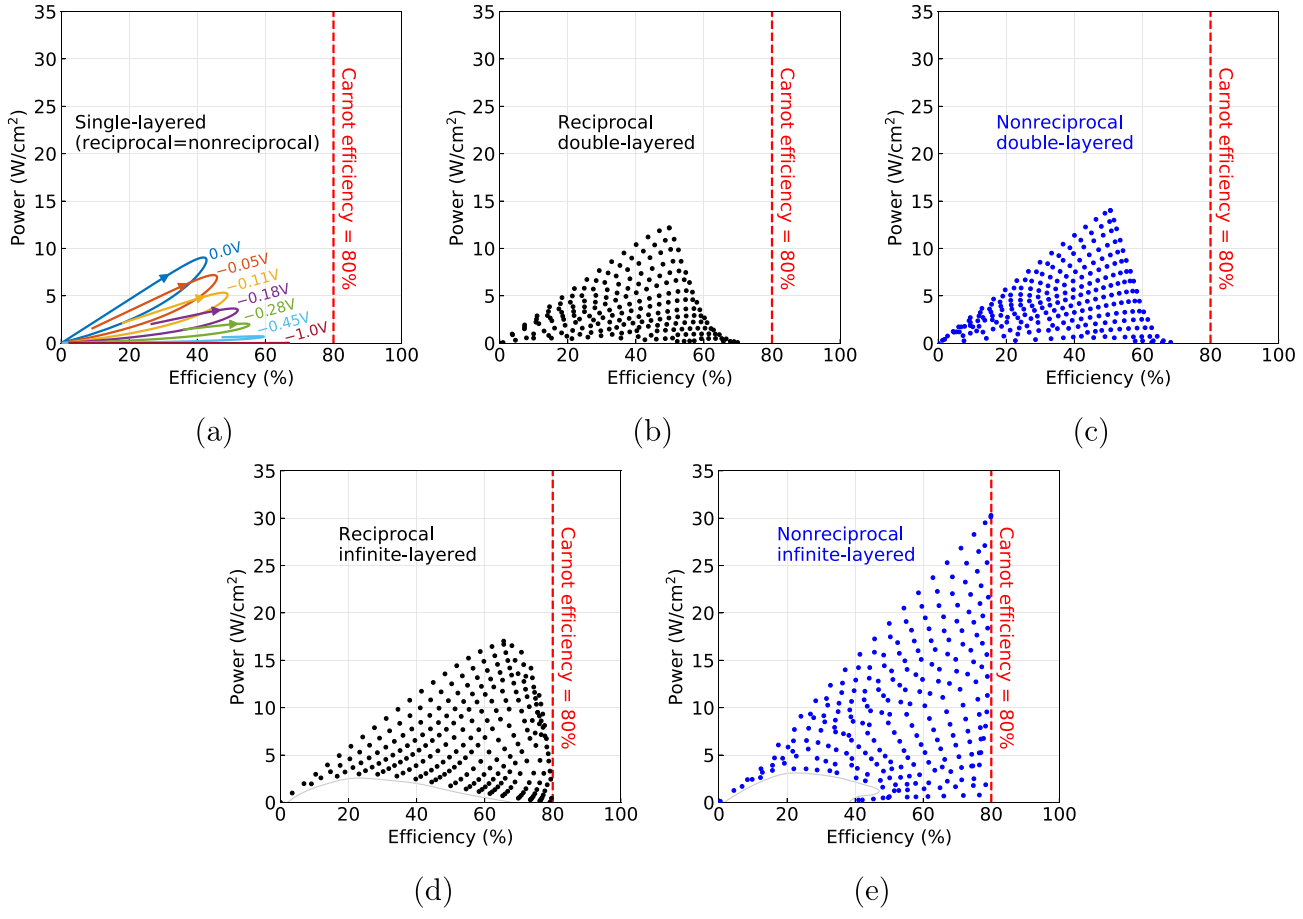

Figure 3. Power vs efficiency plots of various operating conditions (T_H = 1500 K, T_L = 300 K). (a) Single-layered case. Each curve in (a) is obtained by sweeping the operating voltage of the cold side while fixing that of the hot side at the marked values. (b) Reciprocal double-layered case. (c) Nonreciprocal double-layered case. (d) Reciprocal infinite-layered case. (e) Nonreciprocal infinite-layered case. Each point in (b)−(e) represents the power output and efficiency of a certain operating condition.

VARYING OPERATING CONDITIONS

To further elaborate on the relation between power output and efficiency of TPV systems, we show a power vs efficiency plot of various operating conditions in Figure 3. We fix the band gaps at the optimal values determined in the previous section, that is, the band gaps shown in Tables 1 and 2, and we vary the operating voltages of the PV layers. We then observe how the output power and efficiency appear under each operating condition.

Figure 3a shows the plot for the single-layered TPV system (M = 1), in which the operation of nonreciprocal and reciprocal TPV systems is identical. Each curve is obtained by

https://doi.org/10.1021/acsphotonics.2c01308
ACS Photonics XXXX, XXX, XXX−XXX

sweeping the operating voltage of the cold side V_{L1}, while fixing the operating voltage of the hot side V_{H1} at the marked values in the figure. Note that V_{L1} increases in the direction of the arrows in the plot. Initially, the power and efficiency of the system increase with V_{L1}, but as V_{L1} increases further, both the power and efficiency reduce down to zero. Consequently, the area in the power vs efficiency plot that can be covered by all the possible operating conditions becomes limited. We note that this limited area in Figure 3a shows that power output reduces down to zero as efficiency approaches the Carnot limit.

When $M \geq 2$, the trajectory plot obtained by sweeping a single variable like Figure 3a is no longer applicable since there are at least four voltage variables that define an operating condition. Therefore, for multilayered systems, we express each possible operating condition by its corresponding point in the plots. Figure 3b and c show the plots for double-layered systems ($M = 2$), the reciprocal and nonreciprocal case, respectively. Again, for both these cases, areas that can be covered by the possible operating conditions are limited, and in the same way as the $M = 1$ case, power outputs decrease to zero as efficiencies move toward the Carnot limit. These examples of Figure 3a−c show the trade-off between power output and efficiency in finite systems and are in agreement with the work by Shiraishi et al.[24] Another point to note is that in multilayered systems ($M \geq 2$), the nonreciprocal case covers regions with better performance, that is, high-power and high-efficiency regions, compared to the reciprocal case.

Figure 3d and e show the reciprocal and nonreciprocal infinite-layered case ($M = \infty$), respectively, in which the band gap E continuously increases from zero to infinity. For Figure 3d, we tune $V_H(E)$ and $V_L(E)$, which are the operating voltages of the PV layers with band gap E on the hot and the cold side, respectively, following a certain form of function:

$$V_H(E) = \alpha_H\left(1 - \frac{T_H}{T_L}\right)E \tag{8a}$$

$$V_L(E) = \alpha_L\left(1 - \frac{T_L}{T_H}\right)E \tag{8b}$$

where α_H and α_L are coefficients defined for considering various operating conditions. Similarly, in Figure 3e, we tune the operating voltages following the form

$$V_H(E) = V_{H0} + \beta_H\left(1 - \frac{T_H}{T_L}\right)E \tag{9a}$$

$$V_L(E) = \max\left\{0, \beta_L\left(1 - \frac{T_L}{T_H}\right)(E - E_0)\right\} \tag{9b}$$

where β_H and β_L are coefficients defined for varying the functions, and V_{H0}, which is also a variable, is the operating voltage of the leftmost hot side PV layer in Figure 1a. E_0 is the band gap, above which nonzero $V_L(E)$ starts to appear, and this is a variable as well. We note that following the forms of eqs 8a−9b allows us to conveniently avoid thermophotonic operation. In Figure 3d and e, the bottom blank regions appear because the specific function forms of eqs 8a−9b prevent the system from reaching these regions. We believe that if we set $V_H(E)$ and $V_L(E)$ to other reasonable functions, these areas may be filled in. Figure 3d shows that even in the infinite-layered limit, power output from the reciprocal TPV system decreases to zero as Carnot efficiency is reached by tuning the operating condition. On the other hand, as shown in Figure 3e, our nonreciprocal TPV system can attain nonzero power output at Carnot efficiency with an infinite number of layers, which is something that reciprocal systems cannot achieve. Note also that the nonreciprocal case covers far more well-performing operation regions than the reciprocal case.

CONCLUSION

In conclusion, we demonstrate that nonreciprocity can play a significant role in improving the performance of a multi-junction TPV system. We propose a configuration of a nonreciprocal TPV system that can operate at the Carnot efficiency while generating nonzero power in the infinite limit. Even in the case with a finite number of PV layers, as long as our TPV system consists of more than one pair of layers, it outperforms its reciprocal counterpart. Furthermore, by observing the TPV performance under various operating conditions, we show that nonreciprocity is crucial for achieving high efficiency and high power output simultaneously. Considering how little has been explored with regard to applying the concept of nonreciprocity in TPV systems, our work has great potential to provide new opportunities for improving the performance of TPV engines beyond the conventional range.

AUTHOR INFORMATION

Corresponding Authors

Yubin Park − *Department of Electrical Engineering, Stanford University, Stanford, California 94305, United States;* orcid.org/0000-0001-9734-5977; Email: yubinpark@stanford.edu

Shanhui Fan − *Department of Electrical Engineering, Stanford University, Stanford, California 94305, United States; Ginzton Laboratory, Stanford University, Stanford, California 94305, United States;* orcid.org/0000-0002-0081-9732; Email: shanhui@stanford.edu

Author

Zunaid Omair − *Ginzton Laboratory, Stanford University, Stanford, California 94305, United States*

Complete contact information is available at: https://pubs.acs.org/10.1021/acsphotonics.2c01308

Notes

The authors declare no competing financial interest.

ACKNOWLEDGMENTS

Discussions with M. Benzaouia are gratefully acknowledged. This work was supported by the U.S. Department of Energy under Grant DE-FG02-07ER46426.

REFERENCES

(1) Whale, M.; Cravalho, E. Modeling and performance of microscale thermophotovoltaic energy conversion devices. *IEEE Trans. Energy Convers.* **2002**, *17*, 130−142.

(2) Harder, N.-P.; Würfel, P. Theoretical limits of thermophotovoltaic solar energy conversion. *Semicond. Sci. Technol.* **2003**, *18*, S151−S157.

(3) Celanovic, I.; O'Sullivan, F.; Ilak, M.; Kassakian, J.; Perreault, D. Design and optimization of one-dimensional photonic crystals for thermophotovoltaic applications. *Opt. Lett.* **2004**, *29*, 863−865.

(4) Laroche, M.; Carminati, R.; Greffet, J.-J. Near-field thermophotovoltaic energy conversion. *J. Appl. Phys.* **2006**, *100*, 063704.

(5) Park, K.; Basu, S.; King, W. P.; Zhang, Z. M. Performance analysis of near-field thermophotovoltaic devices considering absorption distribution. *J. Quant. Spectrosc. Radiat. Transfer* **2008**, *109*, 305−316.
(6) Rephaeli, E.; Fan, S. Absorber and emitter for solar thermophotovoltaic systems to achieve efficiency exceeding the Shockley-Queisser limit. *Opt. Express* **2009**, *17*, 15145−15159.
(7) Bermel, P.; Ghebrebrhan, M.; Chan, W.; Yeng, Y. X.; Araghchini, M.; Hamam, R.; Marton, C. H.; Jensen, K. F.; Soljačić, M.; Joannopoulos, J. D.; Johnson, S. G.; Celanovic, I. Design and global optimization of high-efficiency thermophotovoltaic systems. *Opt. Express* **2010**, *18*, A314−A334.
(8) Ilic, O.; Jablan, M.; Joannopoulos, J. D.; Celanovic, I.; Soljačić, M. Overcoming the black body limit in plasmonic and graphene near-field thermophotovoltaic systems. *Opt. Express* **2012**, *20*, A366−A384.
(9) Yeng, Y. X.; Chan, W. R.; Rinnerbauer, V.; Joannopoulos, J. D.; Soljačić, M.; Celanovic, I. Performance analysis of experimentally viable photonic crystal enhanced thermophotovoltaic systems. *Opt. Express* **2013**, *21*, A1035−A1051.
(10) Zhao, B.; Wang, L.; Shuai, Y.; Zhang, Z. M. Thermophotovoltaic emitters based on a two-dimensional grating/thin-film nanostructure. *Int. J. Heat Mass Transfer* **2013**, *67*, 637−645.
(11) Bright, T. J.; Wang, L. P.; Zhang, Z. M. Performance of near-field thermophotovoltaic cells enhanced with a backside reflector. *J. Heat Transfer* **2014**, *136*, 062701.
(12) Molesky, S.; Jacob, Z. Ideal near-field thermophotovoltaic cells. *Phys. Rev. B* **2015**, *91*, 205435.
(13) Zhao, B.; Chen, K.; Buddhiraju, S.; Bhatt, G.; Lipson, M.; Fan, S. High-performance near-field thermophotovoltaics for waste heat recovery. *Nano Energy* **2017**, *41*, 344−350.
(14) Fiorino, A.; Zhu, L.; Thompson, D.; Mittapally, R.; Reddy, P.; Meyhofer, E. Nanogap near-field thermophotovoltaics. *Nat. Nanotechnol.* **2018**, *13*, 806−811.
(15) Li, W.; Buddhiraju, S.; Fan, S. Thermodynamic limits for simultaneous energy harvesting from the hot sun and cold outer space. *Light Sci. Appl.* **2020**, *9*, 68.
(16) Mittapally, R.; Lee, B.; Zhu, L.; Reihani, A.; Lim, J. W.; Fan, D.; Forrest, S. R.; Reddy, P.; Meyhofer, E. Near-field thermophotovoltaics for efficient heat to electricity conversion at high power density. *Nat. Commun.* **2021**, *12*, 4364.
(17) Papadakis, G. T.; Orenstein, M.; Yablonovitch, E.; Fan, S. Thermodynamics of light management in near-field thermophotovoltaics. *Phys. Rev. Appl.* **2021**, *16*, 064063.
(18) Omair, Z.; Scranton, G.; Pazos-Outón, L. M.; Xiao, T. P.; Steiner, M. A.; Ganapati, V.; Peterson, P. F.; Holzrichter, J.; Atwater, H.; Yablonovitch, E. Ultraefficient thermophotovoltaic power conversion by band-edge spectral filtering. *Proc. Natl. Acad. Sci. U. S. A.* **2019**, *116*, 15356−15361.
(19) Narayan, T. C.et al.*World record demonstration of > 30% thermophotovoltaic conversion efficiency*. 202047th IEEE Phot. Spec. Conf. 2020; pp 1792−1795.
(20) Fan, D.; Burger, T.; McSherry, S.; Lee, B.; Lenert, A.; Forrest, S. R. Near-perfect photon utilization in an air-bridge thermophotovoltaic cell. *Nature* **2020**, *586*, 237−241.
(21) LaPotin, A.; Schulte, K. L.; Steiner, M. A.; Buznitsky, K.; Kelsall, C. C.; Friedman, D. J.; Tervo, E. J.; France, R. M.; Young, M. R.; Rohskopf, A.; Verma, S.; Wang, E. N.; Henry, A. Thermophotovoltaic efficiency of 40%. *Nature* **2022**, *604*, 287−291.
(22) Burger, T.; Sempere, C.; Roy-Layinde, B.; Lenert, A. Present efficiencies and future opportunities in thermophotovoltaics. *Joule* **2020**, *4*, 1660−1680.
(23) Baldasaro, P. F.; Raynolds, J. E.; Charache, G. W.; DePoy, D. M.; Ballinger, C. T.; Donovan, T.; Borrego, J. M. Thermodynamic analysis of thermophotovoltaic efficiency and power density tradeoffs. *J. Appl. Phys.* **2001**, *89*, 3319−3327.
(24) Shiraishi, N.; Saito, K.; Tasaki, H. Universal trade-off relation between power and efficiency for heat engines. *Phys. Rev. Lett.* **2016**, *117*, 190601.
(25) Park, Y.; Zhao, B.; Fan, S. Reaching the ultimate efficiency of solar energy harvesting with a nonreciprocal multijunction solar cell. *Nano Lett.* **2022**, *22*, 448−452.
(26) Buddhiraju, S.; Santhanam, P.; Fan, S. Thermodynamic limits of energy harvesting from outgoing thermal radiation. *Proc. Natl. Acad. Sci. U. S. A.* **2018**, *115*, E3609−E3615.
(27) Ries, H. Complete and reversible absorption of radiation. *Appl. Phys. B: Laser Opt.* **1983**, *32*, 153−156.
(28) Green, M.*Third Generation Photovoltaics: Advanced Solar Energy Conversion*; Springer Series in Photonics; Springer-Verlag: Berlin, Heidelberg, 2003.
(29) Benenti, G.; Saito, K.; Casati, G. Thermodynamic bounds on efficiency for systems with broken time-reversal symmetry. *Phys. Rev. Lett.* **2011**, *106*, 230602.
(30) Green, M. A. Time-asymmetric photovoltaics. *Nano Lett.* **2012**, *12*, 5985−5988.
(31) Park, Y.; Asadchy, V. S.; Zhao, B.; Guo, C.; Wang, J.; Fan, S. Violating Kirchhoff's law of thermal radiation in semitransparent structures. *ACS Photonics* **2021**, *8*, 2417−2424.
(32) Santhanam, P.; Fan, S. Thermal-to-electrical energy conversion by diodes under negative illumination. *Phys. Rev. B* **2016**, *93*, 161410.
(33) Liao, T.; Zhang, X.; Chen, X.; Lin, B.; Chen, J. Negative illumination thermoradiative solar cell. *Opt. Lett.* **2017**, *42*, 3236−3238.
(34) Ono, M.; Santhanam, P.; Li, W.; Zhao, B.; Fan, S. Experimental demonstration of energy harvesting from the sky using the negative illumination effect of a semiconductor photodiode. *Appl. Phys. Lett.* **2019**, *114*, 161102.
(35) Strandberg, R. Theoretical efficiency limits for thermoradiative energy conversion. *J. Appl. Phys.* **2015**, *117*, 055105.
(36) Martí, A.; Araújo, G. L. Limiting efficiencies for photovoltaic energy conversion in multigap systems. *Sol. Energy Mater. Sol. Cells* **1996**, *43*, 203−222.
(37) Harder, N.-P.; Green, M. A. Thermophotonics. *Semicond. Sci. Technol.* **2003**, *18*, S270−S278.
(38) Wernsman, B.; Siergiej, R.; Link, S.; Mahorter, R.; Palmisiano, M.; Wehrer, R.; Schultz, R.; Schmuck, G.; Messham, R.; Murray, S.; Murray, C.; Newman, F.; Taylor, D.; DePoy, D.; Rahmlow, T. Greater than 20% radiant heat conversion efficiency of a thermophotovoltaic radiator/module system using reflective spectral control. *IEEE Trans. Electron Devices* **2004**, *51*, 512−515.
(39) Burger, T.; Fan, D.; Lee, K.; Forrest, S. R.; Lenert, A. Thin-film architectures with high spectral selectivity for thermophotovoltaic cells. *ACS Photonics* **2018**, *5*, 2748−2754.
(40) Brown, A. S.; Green, M. A. Limiting efficiency for current-constrained two-terminal tandem cell stacks. *Prog. Photovoltaics* **2002**, *10*, 299−307.
(41) Vos, A. D. Detailed balance limit of the efficiency of tandem solar cells. *J. Phys. D: Appl. Phys.* **1980**, *13*, 839−846.

https://doi.org/10.1021/acsphotonics.2c01308
ACS Photonics XXXX, XXX, XXX−XXX